

Detection of CH-53 swashplate bearing deformation - from a 3D dynamic model to diagnostics

Mor Battat¹, Gideon Kogan¹, Alex Kushnirsky¹, Renata Klein² and Jacob Bortman¹

¹*Pearlstone Center for Aeronautical Engineering Studies and Laboratory for Mechanical Health Monitoring, Department of Mechanical Engineering, Ben-Gurion University of the Negev, P.O. Box 653, Beer Sheva 84105, Israel*

*morbat@post.bgu.ac.il
genak@bgu.ac.il
jacobort@bgu.ac.il*

²*R.K. Diagnostics, P.O.Box 101, Gilon, D. N. Misgav 20103, Israel
Renata.Klein@rkdiagnostics.co.il*

ABSTRACT

The purpose of this paper is to present the research approach for the development of an algorithm for detection of a failure of the CH-53 swashplate bearing external spacer. The failure causes a lack of support of the swashplate bearing, thus creating a deformation of the outer ring. This study integrates the results of a new 3D dynamic model, developed for assessment of the defect pattern, and results from experiments. The research approach is planned in hierarchical phases. The experimental phases include a small scale specimen, full scale test rig, helicopter blades test facility and finally a CH-53 helicopter. The unique approach gradually simulates the real work environment of the swashplate bearing. The first two experimental phases and their results are presented. The first experimental phase is conducted on a small scale specimen and the second phase on a full scale test rig. Model results indicate that the lack of support has a defect pattern in both the radial and axial directions. These results are validated with the small scale specimen. In the future phases, the algorithm will be validated with data from the helicopter blades test facility and CH-53 helicopter.

1. INTRODUCTION

In 2008, the swashplate bearings of a CH-53 failed during a flight. The crew, subjected to a stroke followed by significant vibrations, managed to perform an emergency landing. Post-accident examination showed that a failure in the external spacer, separating the duplex ball bearing outer rings, led to collapse of the upper bearing and direct contact

Mor Battat et al. This is an open-access article distributed under the terms of the Creative Commons Attribution 3.0 United States License, which permits unrestricted use, distribution, and reproduction in any medium, provided the original author and source are credited.

between the stationary and rotating swashplate.

The swashplate is a device used for transmitting control inputs to the blades (see Figure 1). Therefore the swashplate bearings are safety of flight critical components. The swashplate of the CH-53 is constructed of two angular contact ball bearings supported by two spacers- internal, between the static inner rings and external, between the rotating outer rings (see Figure 2).



Figure 1. Sikorsky CH-53 swashplate; www.airliners.net

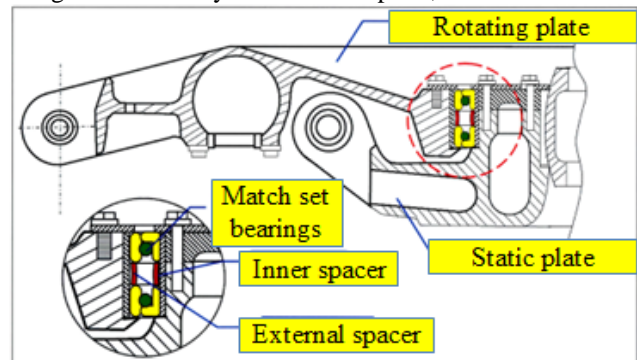


Figure 2. Swashplate cross section

The Laboratory for Mechanical Health Monitoring at Ben Gurion University of the Negev (BGU) is developing a method for early detection of failures caused by deformation of the bearing outer ring and is establishing prognostic tools that could prevent such catastrophic failures.

This article describes the methodology for development of a prognostic tool. The swashplate bearing cannot be efficiently examined before each flight, hence the need to develop a real-time diagnostic tool. The potential benefit of this research results is both in improving the aircraft safety and in reduction of maintenance costs. It should be noted, that the UH-60, as well as other Sikorsky helicopters, have a similar swashplate structure.

The post-accident investigation findings indicate local deflection of the external spacer, adjacent to the grease nipple, as the first stage of the failure. External spacer increased deformation, toward the inner spacer, resulted in abrasion of the two spacers, finally causing the external spacer fracture.

2. GENERAL APPROACH

Pattern of bearings sub-components deformations are not thoroughly investigated, hence the need to study the defects signature. A new 3D dynamic model (Kogan et al., 2012) has been developed as a tool for investigation of faulty bearings behavior. As shown in Figure 3, time history data generated by the model was analyzed in order to define the fault expected pattern. Vibration signals generated by three test systems will be analyzed based on the model results in order to recognize the fault signature. At last, diagnostic algorithms will be applied to vibration data acquired from a CH-53 swashplate. The obtained signature will be compared to the validated dynamic model pattern to define the algorithm and the condition indicators of the fault.

Most bearings dynamic models known today simulate localized faults. Since the majority of used bearings are radial bearings a two dimensional model is sufficient for pattern and behavior simulations. The CH-53 accident examination presents a different case. The axial loading and the fact that the defect is at the supporting spacer rather than at the bearing components requires a new insight.

Constructing a new 3D model was the initial step. The model laid the foundations for the recognition of the defective pattern and the scale of vibrations at different levels of the failure progression. Knowing the expected pattern has a significant advantage when analyzing noisy data.

Comparing the dynamic model results with vibration signals generated by different test systems is planned in phases. It is assumed that when advancing from one phase to another the measured data will simulate more realistically the signal and the environment of the helicopter rotor head. As a result, the difficulty to recognize the pattern of the faulty bearing is

expected to increase from one phase to another, demanding more complex algorithms. Progress in phases is performed to guarantee the recognition of the defect signature among the variety of signals generated by the helicopter during a flight.

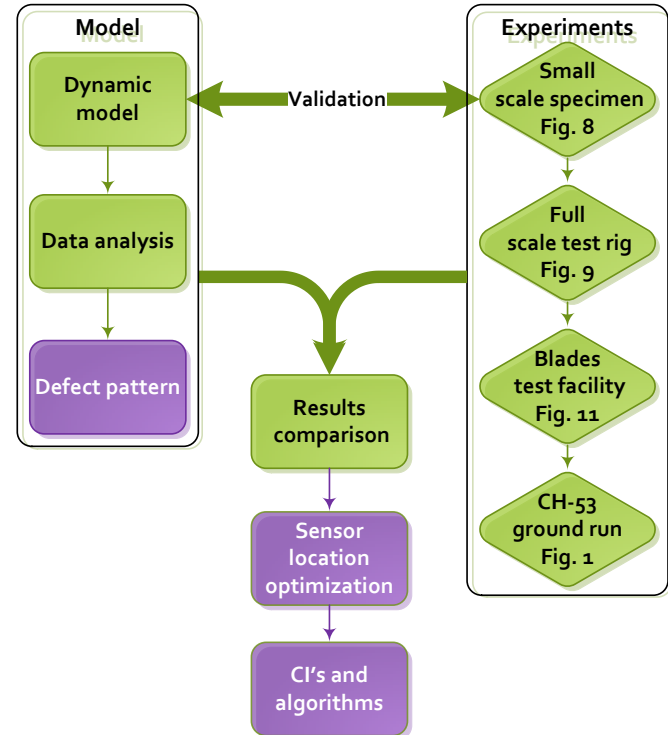


Figure 3. Research flow chart

Two designated test rigs were developed in the BGU lab. A small scale specimen is designed for fast experiments and easy simulation of a wide range of faults. A full scale test rig simulates better the real environment of the helicopter swashplate. The rig, constructed with an original swashplate, provides a good simulation under laboratory conditions of the real support structure. IAI helicopter blades test facility will be a following phase to the laboratory test rigs, simulating a full rotor head including transmission, main shaft and blades. The test systems will be installed and tested with a healthy swashplate at first. After all relevant data is acquired the healthy swashplate will be replaced by a faulty swashplate with a defective external spacer. In the final phase data acquisition will be made on an operational CH-53 ground run. The correlation of the signals between each test system is a primary question of the research and constantly being examined.

Research by Keller & Grabill (2005) examined the detection ability of a CH-47D faulted swashplate bearings by vibration monitoring. The tests were conducted on a swashplate test rig built in back-to-back design in which the upper swashplate assembly is the drive and the lower swashplate assembly houses the tested bearing. The work shows that spalled and corroded bearings are easily

detected. Cage faults, however, were not detected by standard analysis methods.

A paper by Dempsey et al. (2010) compares faulty bearing data collected on a UH-60 Black Hawk helicopters and data collected on a test stand. Three Receiver Operating Characteristic (ROC) curves were used to compare the bearing performances. Variables affecting the ability to recognize a fault are presented. These variables include sensor type, mounting, location, signal processing, structural dynamics, flight regimes, and history of the component. It is concluded that development of diagnostic tools on a test stand is a complicated process due to environmental factors.

Our approach is designed to address the complexity of developing algorithms based on test rig data and implementing the algorithms on data from helicopter flights. The integration of a physical model and hierarchical test systems is a method designed to recognize the fault pattern in the different experimental systems.

Frequently, when analyzing data, appearance of irregular peaks indicates a fault, but one cannot associate the peaks due to lack of the fault pattern. The physical model is a tool aimed to address this uncertainty. The experiment systems are aimed to address the influence of the environmental factors.

3. DYNAMIC MODEL

A new 3D dynamic ball bearing model was developed to study the effect of anomalies in bearing sub-components on the bearing dynamic behavior. The aim of the model is to calculate the dynamic response of a bearing with a wide spectrum of faults. The algorithm was implemented numerically in MATLAB and is based on a model used in a study by Tkachuk and Strackeljjan (2010).

The dynamics, for each bearings component, are based on the classical dynamic equations

$$\Sigma \vec{F}_f + \Sigma \vec{F}_n = m\vec{a}, \Sigma (\vec{R} \times \vec{F}_f) = I\dot{\vec{\omega}}_{xyz} + \vec{\Omega} \times (I\vec{\omega}) \quad (1)$$

where F_f, F_n are respectively the friction and the normal forces that act on a body, with mass m and acceleration \vec{a} ; and $\Sigma(\vec{R} \times \vec{F}_f)$ is the total moment of force acting on a body with a moment of inertia tensor I , angular velocity $\vec{\omega}$; body system xyz , with angular velocity $\vec{\Omega}$; and rotational acceleration, within the body system, $\dot{\vec{\omega}}_{xyz}$.

The relative velocity equation

$$\vec{v}_b = \vec{v}_a + \vec{\omega} \times \vec{ab} \quad (2)$$

Where \vec{v}_x is the velocity of the body at \vec{x} and $\vec{\omega}$ is the angular velocity of \vec{ab} .

The presented equations describe the motion of all the modeled bodies and are solved using time steps (see Figure

4). In each time step, the solution of the equations is based on the previous time step solution, assuming a constant acceleration.

The dynamic model was validated by comparison to analytical solutions and known bearing response to local defects. After validation, the model was implemented for a structural deformation case that corresponds with the accident examination findings.

The failure investigation showed that the external spacer collapse separating the duplex ball bearing outer rings, led to damage of the upper bearing. The deformation of the outer ring was calculated using finite element analysis (see Figure 6). It was found that the lack of proper support causes local deflection in the axial direction of the outer ring of the top bearing. The deflected geometry was implemented in the dynamic model.

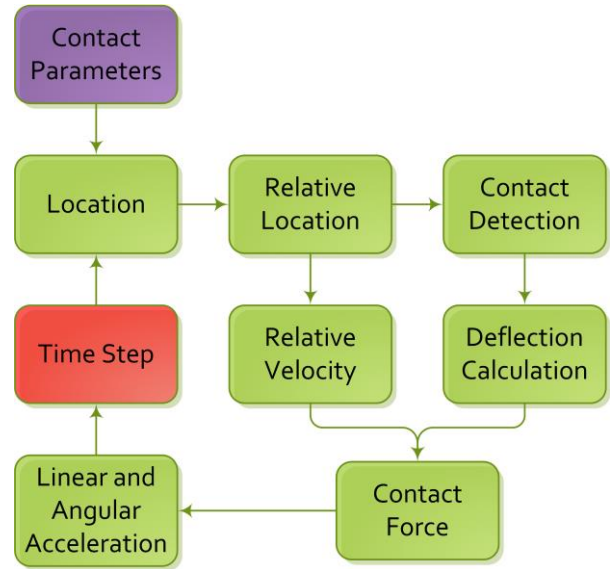


Figure 4. Simplified model algorithm

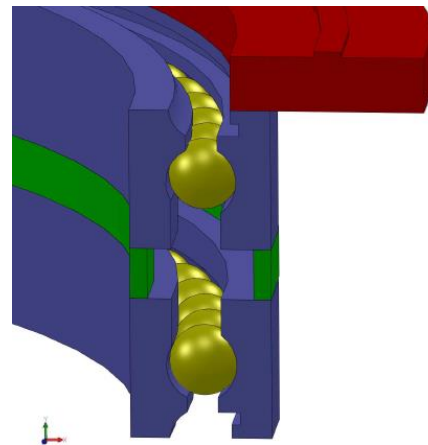


Figure 5. Model section

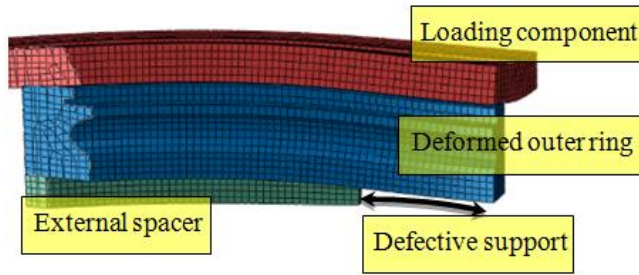


Figure 6. Structural defect finite element model

4. SMALL SCALE SPECIMEN

The small scale specimen is a kit of a generic test rig. The rig, shown in Figure 7, is a versatile platform built to study the signatures of common machinery faults. It has simply operated replaceable kits designed for fast experiments and simulation of a wide range of faults.



Figure 7. Generic test rig with the small scale specimen kit

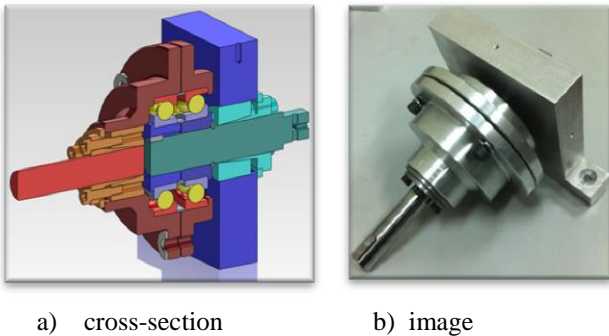


Figure 8. Small scale specimen

The specimen, shown in Figure 8, is constructed of two axial unidirectional ball bearings (NSK 7208BWG) separated by the examined spacers (static internal spacer and dynamic external spacer). The bearings are tightly set into aluminum cups. Pressure, simulating the spacers axial load, is applied by tightening the cups screws, forcing the two outer races onto the spacer.

Experiments included installation of the specimen with a healthy spacer and a number of spacers with faults of different sizes. Variation of tightening pressure resembled the spacers compression. A variable frequency drive controls the velocity of the electric motor and the shaft speed is measured by an optic encoder. Acceleration sensors can be mounted directly to the static shaft or onto the shaft housing, as shown in Figure 8a.

5. FULL SCALE TEST RIG

The main purpose the full scale test rig was to simulate the original work environment of the washplate bearings without the environmental noise. The reduction of noise will help in recognition and isolation of the searched CIs.

The rig, shown in Figure 9, is built around an original CH-53 swashplate. The rotating plate is set in motion by a transmission of gears and a belt driven by an electric motor. The motor is set to rotate the plate at 185 RPM, the CH-53 main rotor speed.



Figure 9. Full scale test rig and sensors locations

Simple and efficient change of swashplates was the main consideration in the design process. Already in-use loading configuration of such test rigs were examined (Bayoumi et al, 2008; Keller & Grabill, 2005). The chosen configuration, shown in Figure 9, has a reduced number of moving parts and lower weight due to reduction of the cyclic loading.

Figure 10 demonstrates the path of the load through the test rig. The simulation of the axial load on the swashplate is done using a hydraulic cylinder. The piston loads the main shaft that transmits the load to the rotating plate through the spider. The rotating plate transmits the load through the bearings to the stationary plate.

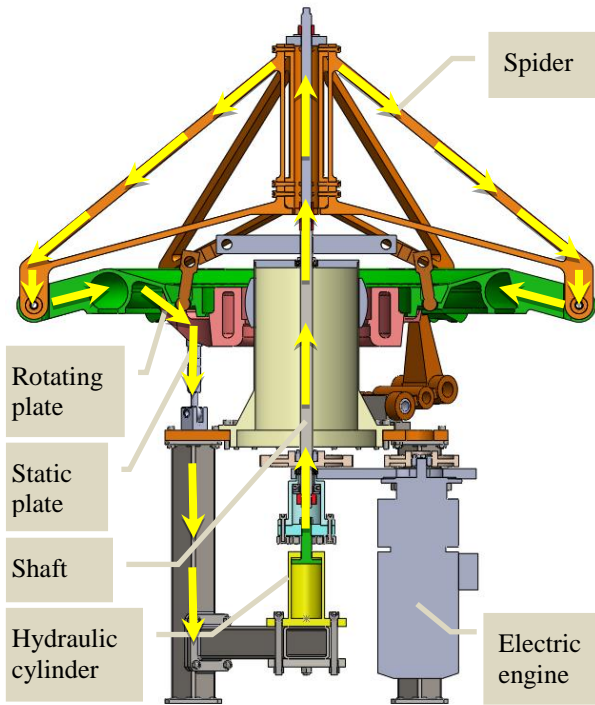


Figure 10. Load transformation over the test rig

In horizontal operating mode the rig simulates hovering due to the symmetric loading, therefore during the first installation, its balance was validated.



Figure 11. Helicopter blades test facility

The experimental program includes runs with healthy and faulty swashplates at a number of rotational speeds, piston

pressures and sensor locations. Five different sensor locations, shown in Figure 9, have been selected considering both operational and scientific applications. The operational locations are derived from helicopter already-in-use sensor brackets and considering maintenance simplicity in case of malfunction. The scientific application considers sensor location optimization and variation of the damping in the rig. Furthermore, transfer function influences the acquired signal. Data from different sensor locations can be used as a tool of comparison or for further analysis.

Experiments at the helicopter blades test facility, shown in Figure 11, are planned to take place in the next phase. For facilitation of data comparison, the same acquisition system and sensors will be used.

6. RESULTS

6.1. Model results

This section describes the model implementation. The model was first designed with the small scale specimen bearing parameters followed by the full scale test rig bearing parameters.

6.1.1. Small scale specimen bearing implementation

The results of the standard bearing (NSK 7208BWG) dynamics under the influence of a defective support are presented. Table 1 presents the bearing parameters.

Table 1. Small scale specimen bearing parameters

Pitch diameter	$60.01 \cdot 10^{-3} [m]$
Ball diameter	$11.91 \cdot 10^{-3} [m]$
Number of balls	14
Outer rings rotation speed	20[rps]
Defect length (azimuth)	30°

During a ball passage through the outer ring deflected zone, the axial load acting on the ball drops and the ball support of the inner ring is reduced. In order to compensate for the support reduction, the neighbor balls are overloaded. The sudden interruption of the inner ring support causes a periodic deflection.

The inner ring center radial acceleration, shown in Figure 12, presents paired impulses that correspond to the impulses of the axial acceleration. However, the impulses that appear in the radial acceleration include shaft speed modulation, which is related to the defect location variation.

The angular distance between the balls is shorter than the angular length of the defect, therefore, between each two impacts corresponding to the interaction of a ball with the fault, appears a third impact that corresponds to next ball entrance into the deflected zone.

Examining the sensitivity of the bearing dynamics to variation of the defect geometry showed that the maximum acceleration of the inner ring is proportional to the maximum outer ring deflection.

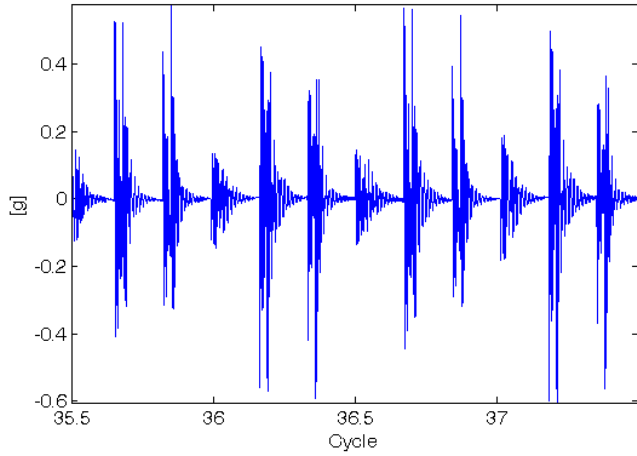


Figure 12. Small scale specimen bearing model results: inner ring radial acceleration

The relation between the outer ring deflected zone length and the bearing dynamics is more complicated. The deflected zone is longer than the angular distance between the balls. Therefore, part of the time, the inner ring is supported by 12 balls. This small period is not enough for stabilization. Therefore, the maximum inner ring center deflection is defined by the length of the period that it is supported by 12 balls. This means that the inner ring center deflection is proportional to the length of the outer ring deflected zone.

The model results show that the acceleration of the inner ring center is a sensitive indicator of the defect existence. Therefore, the power spectral density (PSD) of the simulated acceleration is evaluated for further comparison with the test results.

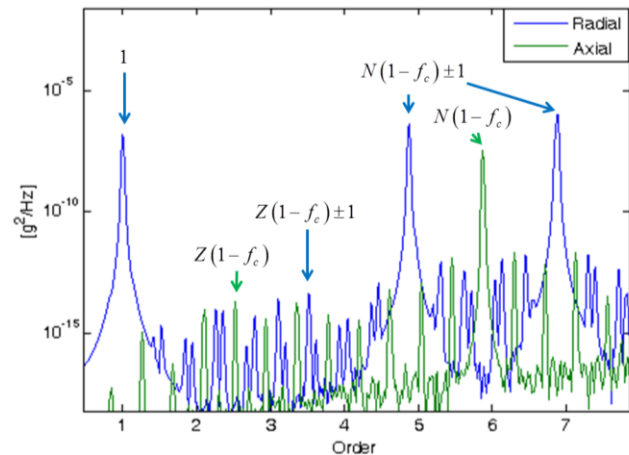


Figure 13. Small scale specimen bearing model results: PSD of the inner ring acceleration

The PSD of the axial acceleration of the inner ring center (see Figure 13) reveals peaks at the order:

$$P_h = Z(1 - f_c) \quad (3)$$

Where Z is an index and f_c is the cage order which is defined as:

$$f_c = \frac{1}{2} \left(1 + \frac{d}{D} \cos(a) \right) \quad (4)$$

The significant peaks of P_h appear when Z is a multiple of number of balls N , i.e. a harmonic of the Ball Pass Frequency Outer race (BPFO).

The spectrum of the acceleration in the radial direction reveals the first harmonic of the shaft speed and peaks at the order:

$$P_s = Z(1 - f_c) \pm 1 \quad (5)$$

The significant peaks of P_s appear when Z is a multiple of the number of the balls, i.e. sidebands of the shaft speed around a harmonic of the BPFO.

6.1.2. Full scale bearing implementation

Implementation of the dynamic model with a CH-53 swashplate bearing parameters was examined. Table 2 presents the bearing parameters.

Table 2. Full scale bearing parameters

Pitch diameter	19.03[in]
Ball diameter	0.5[in]
Number of balls	92
Outer race operational frequency	3.16 [Hz]
Contact angle	30°
Defect length (azimuth)	70°

In agreement with the small scale specimen bearing results the radial direction significant peaks of P_s indicate sidebands of the shaft speed around a harmonic of the BPFO. The axial direction peaks of P_h indicate harmonics of the BPFO. The axial acceleration shows peaks at the BPFO harmonics (44.95, 89.91 ...).

The main parameters affecting the rings acceleration are the number of balls, the axial load and defect length. In order to clearly identify the fault, a relatively large primary defect was produced. As mentioned in Table 2, a defect length of 70° was inserted to the outer spacer.

The effect of the major increase in the number of balls can be seen when comparing the axial acceleration of the small scale specimen bearing (Figure 13) and the full scale bearing (Figure 14).

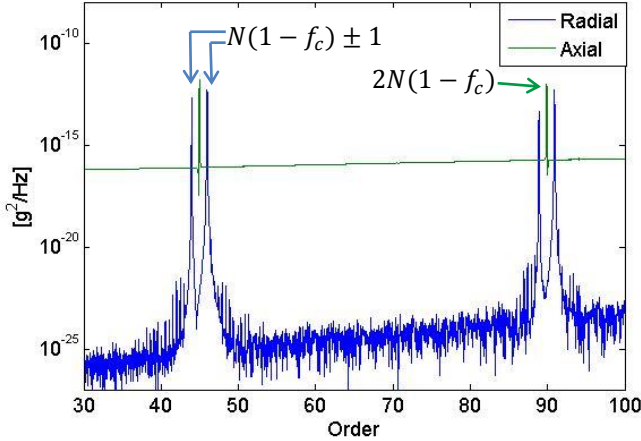


Figure 14. Full scale bearing model results: PSD of the inner ring acceleration

Examination of the model result for various defect lengths is needed. These results would be used for development of a generic failure algorithm independent of the bearing dimensions or the number of balls.

6.2. Small scale specimen experiments

The small scale specimen test results include examination of the fault influence on both radial and axial acceleration spectra (see Figure 15). The comparison between the spectra of the faulty supported bearing in the radial and axial directions reveals that the axial acceleration signal is dominant at the BPFO order harmonics and the radial acceleration signal is predominated by the shaft speed sidebands. These results correspond to the model results presented in Figure 13.

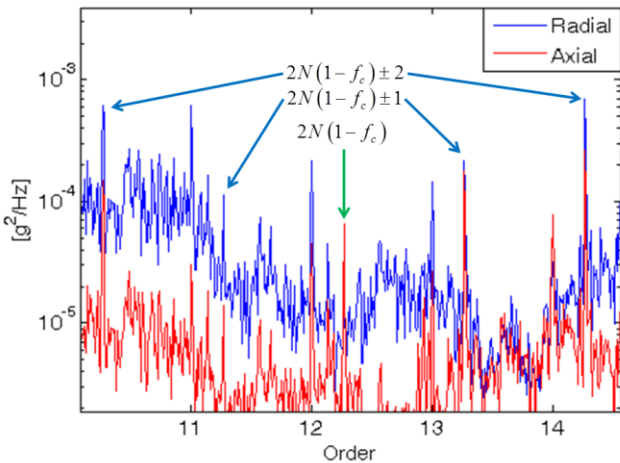


Figure 15. Small scale specimen results: PSD of the faulty supported bearing

The model results, presented in Figure 13, show peaks at orders of $Z(1 - f_c)$ and of $Z(1 - f_c) \pm 1$. When Z is not a multiple of number of balls N , these peaks are low

compared to the BPFO harmonics and to their shaft speed sidebands. Therefore, those peaks cannot be observed in the test results and are probably masked by other sources of vibrations.

6.3. Full scale test rig preliminary results

The rig was tested with a healthy bearing at 185 [RPM] without load. Transmission components frequencies were calculated and identified.

The acceleration PSD of the healthy bearing is presented in Figure 16. The PSD was calculated on the resampled acceleration acquired at sensor location 2 (as shown in Figure 9) in the bearing radial direction. As expected the bearing tones cannot be observed with a healthy swashplate bearing. Compared to the small scale specimen results, it can be seen that the vibration signature contains larger amount of information due to more inputs. This illustrates the expected difficulties in recognizing the pattern in a more realistic environment. Noises resulting from the transmission mask the bearing fundamental frequencies as shown in the multiple peaks appearing around the BPFO second harmonic (89.9). The model results point to the defect location but further analysis is needed in order to recognize the fault in complex mechanical systems.

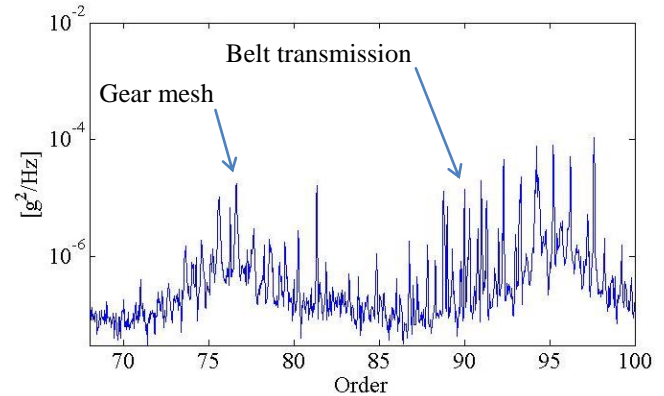


Figure 16. Full scale test rig results: order spectrum of the healthy swashplate acceleration

7. CONCLUSIONS

This paper presents the research approach for the development of an algorithm for detection of a failure of the CH-53 swashplate bearing external spacer. The failure causes a lack of support of the swashplate bearing, thus creating a deformation of the outer ring. This study integrates the results of a 3D dynamic model, developed for assessment of the defect pattern, and results from experimental systems.

The new dynamic model predicts a defect pattern for the unique, newly-researched failure. The results present the defect pattern in the radial and axial directions. A similar

schematic pattern was obtained in both the small scale specimen bearing and the full scale bearing. This pattern can be used in the future to develop a generic algorithm for detection of the failure independent of the bearing dimensions or the number of balls.

The small scale specimen is designed for fast experiments and easy simulation of a wide range of faults. Experiments of the small scale specimen simulating the fault are in good agreement with the model results.

A full scale test rig was constructed to simulate more realistically the signals generated by the rotating swashplate. The test rig configuration allows swashplates to be easily replaced and operated. The test rig was constructed to function under a static load and rotational speed of an operational main rotor while keeping a low number of moving parts and using a small electric motor. Preliminary experiments conducted on the test rig confirm the increase in noise sources. The appearance of multiple peaks around the BPFO second harmonic observed in the test rig experiment illustrates the need to integrate the model results with experiments.

In the next steps it is planned to complete the seeded fault tests on the full scale test rig and examine the algorithm with data from the helicopter blades test facility and the CH-53 helicopter.

ACKNOWLEDGEMENT

We gratefully acknowledge the invaluable support of Dr. Avi Weinreb and Tal Yehoshua.

We would also like to thank the Perlston Foundation.

REFERENCES

- Kogan, G., Bortman, J., Kushnirsky, A. & Klein, R. (2012). Ball bearing modeling for faults simulation. *The Ninth International Conference on Condition Monitoring and Machinery Failure Prevention Technologies* (no. 1, pp. 1–8).
- Tkachuk, P. & Strackeljan, J. (2010). A 3D-ball bearing model for simulation of axial load variations. *The Seventh International Conference on Condition Monitoring and Machinery Failure Prevention Technologies* (pp. 1–10).
- Keller, J. & Grabill, P. (2005). Inserted fault vibration monitoring tests for a CH-47D Aft swashplate bearing. *The American helicopter society 61st Annual Forum*.
- Bayoumi, A., Goodman, N., Shah, R., Roebuck, T., Jarvie, A. & Eisner, L. (2008). Conditioned-Based Maintenance at USC - Part III: Aircraft Components Mapping and Testing for CBM. *The American Helicopter Society Specialists' Meeting on Condition Based Maintenance*. Huntsville.
- Blechertas, V., Bayoumi, A., Goodman, N., Shah, R. & Shin, Y. J., (2009). CBM Fundamental Research at the

University of South Carolina: A Systematic Approach to U.S. Army Rotorcraft CBM and the Resulting Tangible Benefits. *The American Helicopter Society Technical Specialists' Meeting on Condition Based Maintenance*. Huntsville.

- Chin, H. H., Mayhew, E. & Green, D. L. (2005). Assessing Bearing Health for Helicopter Power Train Systems. *American Helicopter Society 61st Annual Forum*. Grapevine.
- Blunt, D. M. & Keller, J. A. (2006). Detection of a fatigue crack in a UH-60A planet gear carrier using vibration analysis. *Mechanical Systems and Signal Processing*, 20(8), 2095–2111.
- Dempsey, P., Branning, J. & Arsenal, R. (2010). Comparison of Test Stand and Helicopter Oil Cooler Bearing Condition Indicators. *AHS 66th Annual Forum and Technology*.
- Budynas, R. & Nisbett, K. (2006). Shigley's Mechanical Engineering Design (*Mcgraw-Hill Series in Mechanical Engineering*). McGraw-Hill Science/Engineering/Math.